Acoustic Emission in Fracture of Structural Materials With Non-metallic inclusions

KANJI ONO and H. B. TEOH*

Department of Materials Science and Engineering, School of Engineering and Applied Science, University of California, Los Angeles, California 90024-1595, USA

**Now at Digital Equipment Corp., Andover, Massachusetts 01810-1098, USA*

Abstract

The acoustic emission (AE) behavior of structural materials during fracture testing was investigated. Slow-bend tests were performed using heat treated Charpy V-notch samples of A533B steels. From AE measurements and post-test fractographic analysis, the AE signals associated with various fracture mechanisms were classified on the basis of peak amplitude. Tear and shear fractures and dimple formation by microvoid coalescence generated low-amplitude AE events. Quasi-cleavage and cleavage fractures emitted events with a broad range of amplitudes. Decohesion of MnS inclusions generated AE events with the amplitude distributions of Weibull type. When the decohesion occurs, AE events from this process mask those from plastic deformation or from tear, shear or microvoid coalescence; only quasi-cleavage or cleavage fracture can be distinguished by peak amplitudes.

Keywords

Acoustic emission; fracture mechanisms; A533B steels; amplitude distribution analysis.

Introduction

Previous studies have indicated that structural steels exhibit anisotropic acoustic emission (AE) behavior during deformation and fracture (Ono et al., 1976; Ono and Yamamoto, 1981). Such AE behavior is due to the presence of nonmetallic inclusions. During tensile and fracture tests, samples of short-transverse orientations (S- and ST-orientations in terms of ASTM designation) emitted burst-type AE signals which persisted from the elastic-loading region to maximum load. The sources of the signals are the decohesion of elongated MnS inclusions. Samples of L- and LT-orientations (longitudinal orientations) produced much lower AE activities essentially consisting of continuous-type and were prominent only at general yield with few burst emissions. These AE activities were due to plastic deformation. Certain ductile fracture mechanisms also contributed to observed burst-type AE at higher load levels.

To understand the fracture-induced AE and their origins, three-point bend tests of A533B steel were performed in this study. Fractographic examination of this steel revealed various fracture processes (Teoh and Ono, 1987). AE measurements during such tests reveal AE signals with a variety of peak amplitude distribution characteristics. In order to correlate fracture mechanisms and the AE signals they emit, interrupted tests were conducted. Tests at -75 to +150°C were also conducted. From AE measurements and post-test fractographic analysis, the AE signal characteristics associated with each fracture mechanism were then identified.

Material and Experimental Procedures

The material used in this study is a low-alloy ASTM A533B class 1 steel of 165 mm thickness. The chemical composition is C: 0.18, Si: 0.25,.Mn: 1.43, P: 0.013, S: 0.005, Mo: 0.50, Ni: 0.66, Cr: 0.28, Cu: 0.01 (in wt. %). Standard Charpy V-notch (45°) specimens were employed with or without pre-crack. Two specimen orientations were selected: LT and ST. The specimens were given one of three heat treatments: quenched (930°C,

1 hr, oil-quenched), quenched and tempered (930°C, 1 hr, oil-quenched + 650°C, 24 hr, oil-quenched), and normalized and tempered (930°C, 1 hr, air-cooled + 650°C, 24 hr, furnace-cooled).

Most mechanical tests were performed at room temperature on a floor-model Instron testing machine at a constant crosshead speed of 0.021 mm/s. Test temperature ranged from -75° to 150°C. The AE parameters evaluated were cumulative AE event counts, rms voltage and peak amplitude distribution of AE signals. AE measurements were obtained using a 175 kHz resonant transducer (AET Corp. AC 175L) and a preamplifier (60 dB gain) with 125-250 kHz filter. The transducer was coupled to one end of the Charpy specimen using wax. For low temperature tests, a stainless steel waveguide was soldered to one end of the specimen and the transducer was kept outside the cold chamber. A true rms voltmeter (HP 3400A) provided the rms voltage data. AE event count measurements and peak amplitude distribution analysis were obtained using a microcomputer-based AE instrumentation (AET Corp. Model 5000) and an amplitude distribution analyzer (AET Corp. Model 203). The input noise level was 1.4 μV at the preamplifier input. The threshold value for both Model 5000 and Model 203 was 15 μV, corresponding to 24 dB (0 dB refers to 1 μV). The amplitude level in dB will be referenced to 1 μV. After testing, unfractured samples were broken by impact at -196°C to reveal the fracture surfaces. The fractured samples were examined using a Cambridge Stereoscan 2150 scanning electron microscope (SEM) operating at 20 kV.

Results and Discussion

Tear/Shear Mechanisms

The load-time curves for quenched samples in the LT and ST orientations tested at 23°C are given in Figs. 1a and 1b. The quenched sample in the LT orientation fractured soon after reaching the maximum load as shown in Fig. 1a. The quenched ST sample fractured right at the maximum load (see Fig. 1b). Also shown are the rms voltages of AE signals and the cumulative AE event counts (marked as AE and N, respectively). In both orientations, the rms voltage plots indicate small increases due to plastic flow. When the load reached 28 to 29 kN, strong burst emissions were observed. Before this sudden increase, AE event counts increased slowly to 80 (LT) or 350 (ST). High AE levels continued to fracture. Note that the full scale of the rms voltage was increased one-hundred fold to 1 mV in this region. Reflecting a greater deflection to fracture in the LT-orientation sample, the total event count was 50 % higher in the LT-sample than in the ST-sample.

The fracture surface of the quenched LT sample showed that crack initiation occurred at machining marks at the notch root and a well-developed stretch zone extended from the notch root for 40 and 60 μm. It was followed by a region containing large shear dimples which are separated by finer, equiaxed dimples due to microvoid coalescence. In other areas, isolated colonies of quasi-cleavage facets followed the stretch zone. These facets, which occurred at 100 - 200 μm from the notch root, were arrested after running for a distance of about 100 μm. Most of the fractures described above were also found in the quenched ST sample. However, the fracture surface of this sample also contained numerous elongated MnS inclusions. These inclusions lie parallel to the crack front.

The fracture surface of another quenched LT sample that was loaded to general yield (equivalent to Point 1 of Fig. 1a) revealed elongated dimples initiating from multiple sites at old machining marks. The cusps of these severely distorted dimples point towards the notch (on both faces), suggesting that they were formed by a tearing mechanism. The stretch zone ended abruptly, and was followed by a zone of fibrous rupture. Within this zone, there exists a bimodal distribution of shear dimples: larger, elongated dimples with diameters between 50 to 100 μm and smaller, also elongated dimples with diameters of about 1 μm. Except for a small number of the large dimples, the finer dimples covered almost the entire fibrous zone.

The tear and shear fracture mechanisms were associated with low level AE signals. The rms voltage rose immediately above the background level (1.4 μV at the transducer) as loading began. It increased slightly to about 1.7 μV at general yield. Amplitude distribution of AE signals for this pre-yield region is shown in Fig. 2. Most events have amplitudes that centered around 30 dB. Cumulative amplitude distribution can be roughly approximated by power-law distributions of the form (Nakamura et al., 1971; Pollock, 1973; Ono and Yamamoto, 1981),

$$N = A\,(V_p)^{-n} \qquad (1)$$

where N is the cumulative event count, V_p is the peak amplitude, A and n are constants. The data in Fig. 2 may be fitted with this equation having the exponent of 1.8. However, the observed distribution can be better represented by two Weibull distributions. The Weibull function is usually given as

$$N = C \exp\left(-D\,(V_p)^{q}\right) \qquad (2)$$

where C, D and q are constants. Here, two dotted curves in Fig. 2 have the exponents of 4 (lower amplitude) and 1.2 (higher amplitude), respectively. Typically, the exponent of 4 corresponds to the distribution due to continuous emissions from plastic deformation.

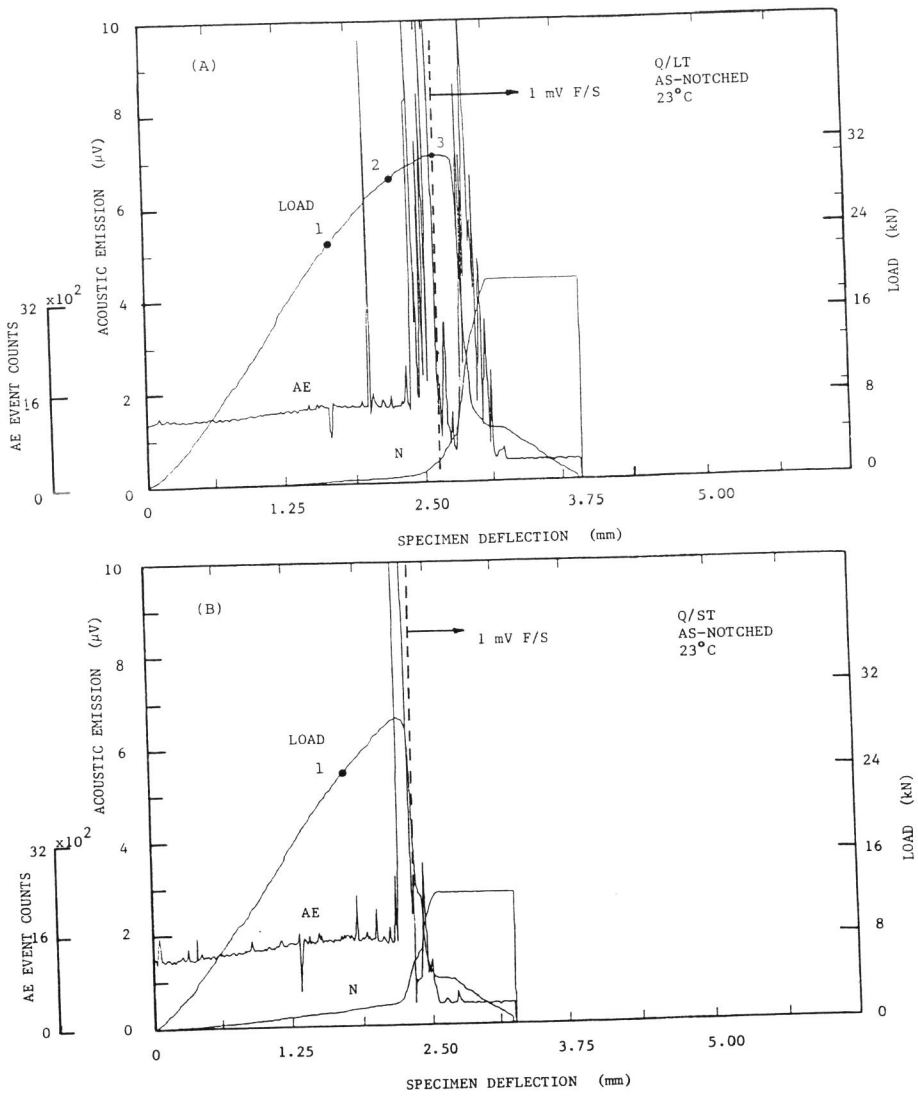

Fig. 1 Load and AE data plotted against specimen deflection for the three point bend tests of quenched samples. (a) For a quenched LT-orientation sample. (b) For a quenched ST-orientation sample.

When another quenched LT sample was loaded past general yield (to Point 2 in Fig. 1a), the additional deformation beyond general yield affected the stretch zone that had been formed earlier. The post-yield deformation smoothed out or even destroyed some of the dimples which formed earlier during crack initiation. The stretch zone merged into a region consisting of a combination of large, deep shear dimples and finer, shallower equiaxed dimples. Slip markings appeared especially on the walls of the large dimples, reflecting the extensive plastic deformation that occurred during the crack growth process. Many voltage spikes accompanied

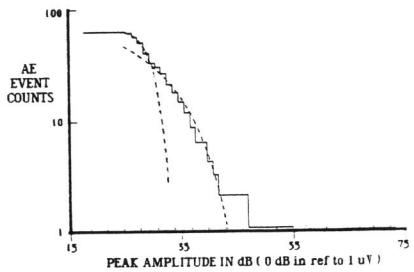

Fig. 2 Cumulative peak amplitude distribution of AE events for quenched LT orientation sample loaded to general yield.

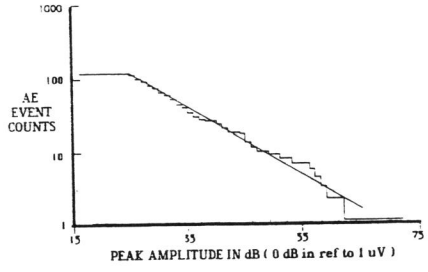

Fig. 3 Cumulative peak amplitude distribution of AE events for quenched LT orientation sample loaded to beyond general yield.

this decrease. Amplitude distributions of the AE signals (cf. Fig. 3) indicate that most events have low amplitudes, 90% of which occurring below 45 dB. The stronger emissions above 45 dB must have arisen from fracture processes which occurred beyond general yield. The cumulative amplitude distribution can be approximated by the power-law (equation 1), with the exponent of 0.85.

During crack initiation and propagation involving tear or shear fracture of quenched LT samples of A533B steel emitted low-amplitude events. Their peak amplitudes were generally below 47 dB. The cumulative amplitude distribution can best be represented by the power-law with the exponent of 0.85 to 1.8.

Quasi-cleavage Fracture

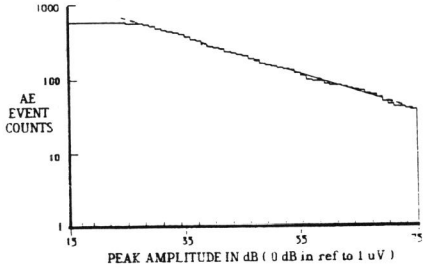

Fig. 4 Cumulative peak amplitude distribution of AE events for quenched LT orientation sample loaded to fracture.

The fracture surfaces of quenched LT samples which were loaded to past maximum load (Point 3 in Fig. 1a) or to failure reveal the presence of quasi-cleavage facets beyond the slow crack growth region. The facets occurred in isolated colonies and were arrested after running for distances up to about 100 μm. Near the maximum load, the rms voltage curves of these samples displayed energetic rms voltage spikes. Some of these spikes peaked at 1 mV (at the transducer) on the rms voltage curve. Amplitude distributions of AE signals indicate that large-mplitude events accompanied athe voltage spikes. As evident in Fig. 4, the peak amplitudes now spanned the range from 27 dB to the maximum amplitude measured. This contrasts with peak amplitudes below 47 dB for AE from a similar sample loaded to general yield (cf. Fig. 2). Events with amplitudes above 54 dB led to a decrease in the slope of the power-law distribution of AE events to a value of 0.5. However, note that AE signals for the quenched LT sample loaded to fracture also caused a general increase in the number of events with lower amplitudes (cf. Figs. 2 and 3). The overall effect is indicated most clearly by the cumulative event counts in Fig. 1a for the quenched LT sample that was tested to failure. The figure indicates that AE events which occurred beyond the maximum load accounted for about 85% of the total event counts for the sample. That is, the largest increase in event counts took place during the falling load period. From fractographic evidence, quasi-cleavage fracture must have generated the high-amplitude AE events mentioned here.

The correlation between quasi-cleavage fracture and large-amplitude AE events is not surprising and is consistent with results reported in the literature (Ringshall and Knott, 1978; Khan et al., 1982; Ringshall et al., 1980). For instance, Khan et al. (1982) studied the initiation and propagation of cleavage microcracks using peak amplitude analysis in two turbine rotor steel forgings and AISI 4340 steel. In the early stages of fracture testing, AE signals with peak amplitudes less than 0.5 mV or 54 dB (at the transducer) were observed. Immediately before final fracture of the sample, a large number of energetic signals were emitted for short durations. These have peak amplitudes greater than 2 mV (66 dB) and are associated with cleavage microcrack growth that led to final unstable fracture. During transgranular cleavage fracture in a high nitrogen mild steel, Ringshall and Knott (1978) reported that individual events often have amplitudes exceeding 100 mV (100 dB) at the transducer. They

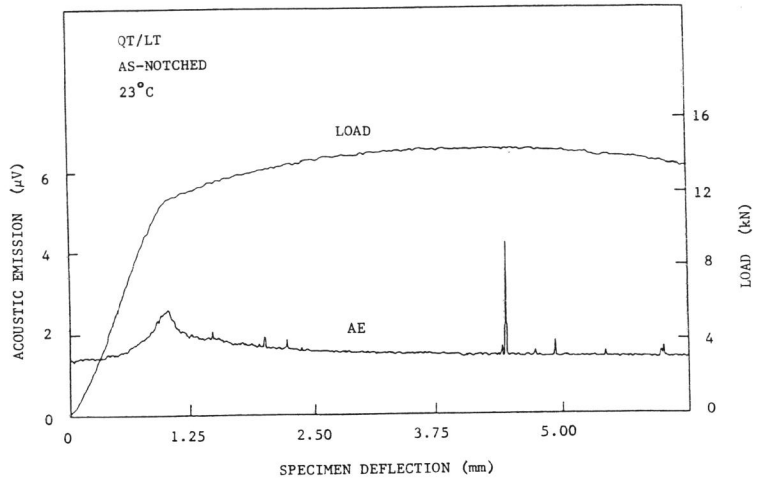

Fig. 5 Load and AE data for quenched and tempered (650°C/24 hr) LT-orientation sample.

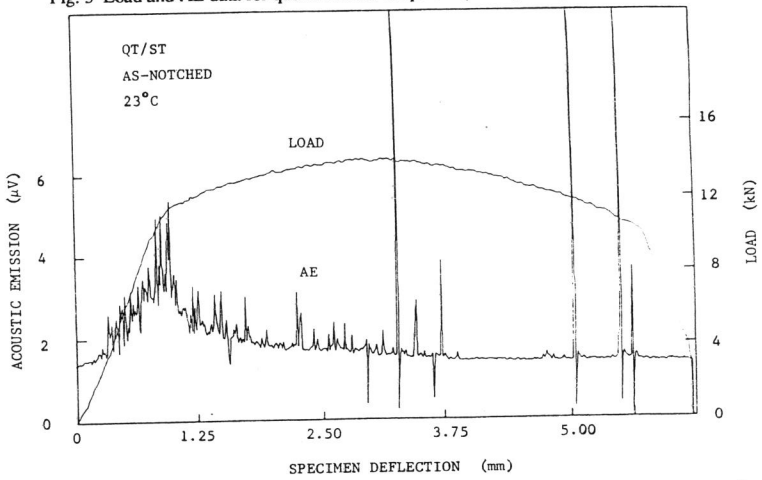

Fig. 6 Load and AE data for quenched and tempered (650°C/24 hr) ST-orientation sample.

attributed this phenomenon to the cleaving of several grains at the same time. In A533B steel, Ringshall et al. (1980) associated AE with peak amplitudes greater than 1.5 mV (or 63.5 dB) to isolated cleavage areas which were induced by prestraining.

Microvoid Coalescence

The load data for quenched and tempered samples in the LT and ST orientations are given in Figs. 5 and 6. Here, the load-time curves exhibited a sharp transition at general yield. Tempering of quenched samples reduced both the general yield and maximum load levels. However, the total deflection to maximum load increased substantially. Another important difference between the quenched and quenched and tempered samples is that the latter did not fracture macroscopically during test. Like its quenched counterpart, the quenched and tempered ST sample reached its maximum load much sooner than the quenched and tempered LT sample and exhibited lower total deformation. The fracture surface of the quenched and tempered LT sample is characterized by a fibrous crack

in the form of a thumbnail in the center of the specimen where the maximum constraint existed. On both sides of the fibrous crack were ligaments of about 2 mm width. A stretch zone extended across the central two-thirds of the crack front, terminating at the side ligaments. Its average width is about 100 μm. Large, oval-shaped craters, indicating sites once occupied by inclusions, are distributed generously within the fibrous zone. The remaining surface of the fibrous zone is covered with fine dimples, consisting of ductile dimples between 1 and 2 μm diameter, formed by microvoid coalescence. Some dimples contained fine inclusions of less than 0.2 μm size. Some secondary cracks are also observed.

The fracture surface of the quenched and tempered ST sample is also characterized by a thumbnail-fibrous crack in the center of the specimen. The fibrous zone is separated from the notch tip by a region of shear cracks. In addition, it is covered almost entirely by large inclusion troughs, some of which were 1 mm long. Many of the troughs also contain smaller inclusion-nucleated voids within them.

Tempering of quenched samples led to sharpening and an increase in peak value of the rms voltage curve. This is evident in Fig. 5 for the quenched and tempered LT sample. The rms voltage curve peaked at 2.6 μV at general yield. Beyond general yield, the rms voltage curve decreased, but more sharply than quenched samples did. Further loading caused a steady decrease in rms voltage, but at a rate more gradual than the initial decrease that occurred immediately after general yield. The rms voltage dropped to near background level at maximum load. Unlike the quenched samples, the quenched and tempered LT sample did not generate any large amplitude AE signals.

The AE associated with dimple fracture consists of low amplitude emissions as evident in the amplitude distribution shown in Fig. 7. The emissions have peak amplitudes between 27 and 47 dB, with a majority with amplitudes below 39 dB. This range of peak amplitude is similar to that due to plastic deformation. The cumulative amplitude distribution can be represented by the power-law function with an exponent of 1.7.

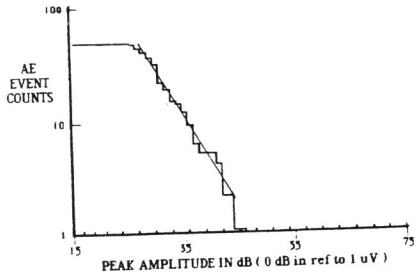

Fig. 7 Cumulative peak amplitude distribution of AE events for a quenched and tempered LT orientation sample loaded to the maximum load.

Decohesion of MnS Inclusion

As in the case of the quenched and tempered LT sample, the macroscopic fracture surface of a quenched and tempered ST sample is characterized by a fibrous crack in the form of a thumbnail in the center of the notch. The fibrous crack was covered completely by large inclusion-induced troughs, however, and some of them were 1 mm long. Most of the inclusions have been identified as MnS and are visible in Fig. 8.

The quenched and tempered ST sample generated burst emissions which are associated with the decohesion of MnS inclusions. The AE behavior was active and was represented by numerous spikes on the AE rms voltage curve which began as soon as loading of the sample commenced (see Fig. 6). The AE activity reached a peak at general yield and it persisted to the maximum load. The average height of the rms voltage spikes decreased with increasing amount of sample deflection beyond general yield. The active AE behavior of the quenched and tempered ST sample was also indicated by the cumulative event count, which increased rapidly in the elastic-loading region of the test. With further loading, the event counts continued to increase but at a reduced rate. The total count at maximum load was 2500 events.

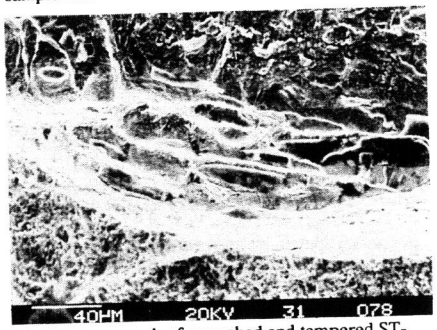

Fig. 8 Fractograph of quenched and tempered ST-orientation sample showing MnS inclusions aligned parallel to the fracture surface.

The peak amplitudes of the burst emissions lie in the range between 27 and 54 dB, which remained constant for the duration of the test. However, a majority of the AE events actually have peak amplitudes below 34 dB. Figure 9 reveals that the cumulative peak amplitude distribution of the AE events in the elastic-loading region can be described by a Weibull distribution (equation 2) characteristic of MnS inclusion decohesions (Ono et al., 1978; Ono and Yamamoto, 1981). The distribution in Fig. 9 has an exponent q = 0.35. However, when the

loading was continued to higher load levels, burst AE from the decohesion of MnS inclusions started to diminish. In combination with deformation beyond general yield, the cumulative amplitude distributions were better represented by the power-law function of equation 1. The slopes of the curves remained approximately constant at 1.5 throughout the remainder of the test.

The behavior of the cumulative distribution of AE signals of the quenched and tempered ST sample just described is slightly different from that of as-received or normalized and tempered (650°C) samples of the same orientation (Okajima and Ono, 1980; Ono and Yamamoto 1981). Those samples were characterized by a single amplitude distribution function for the duration of the test, namely, the Weibull function of equation 2 with exponents between 0.3 and 0.4. The dominance of a single function suggests the operation of a single AE source, i.e., the decohesion of MnS inclusions.

In the present study, amplitude distribution analysis of AE events indicates that the decohesion of MnS inclusions accounted for most of the AE events detected only during the elastic loading of the sample. With larger sample deflection, the decohesion of MnS inclusions still contributes to the AE observed, but other sources also operate, leading to a slight modification of the amplitude distributions.

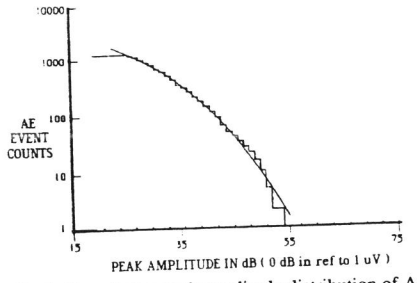

Fig. 9 Cumulative peak amplitude distribution of AE events for a quenched and tempered ST orientation sample, showing the characteristic Weibull distribution with q = 0.35 (eqn 2).

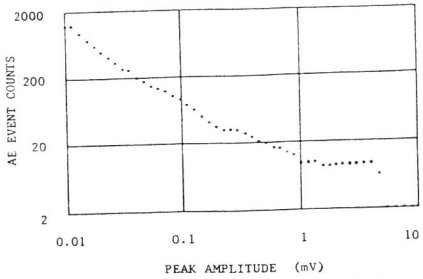

Fig. 10 Cumulative peak amplitude distribution of AE events for a normalized and tempered ST orientation sample.

Cleavage Fracture

The fracture surface of a normalized and tempered ST sample tested at -75°C shows cleavage facets with some ductile tearing. The sample failed during test at a load slightly above general yield. The cumulative distribution of AE signals of this sample, Fig. 10, indicates the presence of AE events with peak amplitudes up to the maximum measured. Events with amplitudes above 1 mV (60 dB) differentiate this distribution from the characteristic Weibull distribution of MnS inclusion decohesion. The high amplitude events (> 1 mV) accounted for about 15 to 70% of the total event counts for normalized and tempered samples tested at low temperatures. These occurred during a jump in the total event counts during the falling load period. However, there was a major difference in the mode of crack propagation after cleavage crack initiation in quenched and normalized and tempered samples. In the quenched samples, which were tested at room temperature, there was a fracture mode conversion from quasi-cleavage to dimple formation by microvoid coalescence beyond maximum load. On the other hand, the normalized and tempered samples tested at -75°C fractured unstably by cleavage. Nevertheless, both cleavage and quasi-cleavage generated high-amplitude AE events.

Summary and Conclusions

From AE measurements and post-test fractographic analysis, the ranges of peak amplitudes of AE events from various fracture mechanisms in A533B steel were identified. The results indicated that tear/shear fracture emitted low-amplitude events, with amplitudes below 47 dB. Due to the low levels of continuous AE signals, as indicated by the rms voltage curves, when compared to the threshold value selected (15 μV at the transducer), the events detected represented mostly burst emissions.

The observation of the correlation between AE and tear and shear fracture in samples with different orientations or heat treatments suggests that it may be common to many ductile cracking processes which involve tear and shear. However, the results also reveal a limitation in the use of AE technique to detect slow crack initiation and growth: the AE events from tear and shear fracture as well as microvoid coalescence have peak amplitude range similar to that from plastic deformation. Therefore, it would be difficult to differentiate these fracture processes

(tear, shear or microvoid coalescence) from plastic deformation based on peak amplitude. However, when cleavage or quasi-cleavage fracture occurs, large-amplitude AE events are emitted and can be detected easily.

Decohesion of MnS inclusions generated events with amplitudes up to 54 dB and their amplitude distributions show the characteristic Weibull distribution. When decohesion occurs, AE events from this process would mask those from plastic deformation or fracture processes such as tear, shear or microvoid coalescence; only cleavage or quasi-cleavage fracture may be separated based on peak amplitudes of AE events.

The findings are summarized below:

Fracture processes during three-point bend tests of A533B steel were correlated to the AE signals they emitted.

Tear or shear fracture and dimple formation by microvoid coalescence generated AE events with peak amplitudes typically below 47 dB.

Quasi-cleavage and cleavage processes emited events with a broad range of amplitudes, including events with high amplitudes well above
54 dB.

Decohesion of MnS inclusions generated AE events with peak amplitudes up to 54 dB and with amplitude distribution having the characteristic Weibull distribution.

When inclusion decohesion occurred, the AE events from this process completely masked and obscured those due to tearing, shear-cracking and dimple fracture.

Ackowledgement

This research was supported by the Office of Naval Research. The steel plate used was supplied by Nippon Steel Corp. through the courtesy of its Los Angeles Office.

References

Khan, M.A., T. Shoji and H. Takahashi (1982), Metal Science, **16**, 118-126.

Nakamura, Y., C.L. Veach and B.O. McCauley (1971), Acoustic Emission, ASTM STP 505, Amer. Soc. for Testing and Materials, Philadelphia, pp. 164-186.

Okajima, K. and K. Ono (1980), Proc. 5th Acoustic Emission Symp., Japan Soc. NDI, Tokyo, pp. 270-281.

Ono, K. and M. Yamamoto (1981), Mat. Sci. Engr., **47**, 247-263.

Ono, K., H. Hatano and G. Huang (1976), Proc. 8th World Conf. on Nondestructive Testing, Cannes, France, Conference Secretariat, Paris, Sec. 3K3, pp. 1-10.

Ono, K., R. Landy and C. Ouchi (1978), Proc. 4th Acoustic Emission Symp., Int. Tech. Exchange Center, Tokyo, pp. 4/33-4/45.

Pollock, A.A. (1973), Non-Destructive Testing, **6**, 264.

Ringshall, N.W., and J.F. Knott (1978), Proc. 4th Acoustic Emission Symp., Int. Tech. Exchange Center, Tokyo, pp. 8/1-8/23.

Ringshall, N.W., K. Okamoto, T. Nakamura and J.F. Knott (1980), Proc. 5th Int. Acoustic Emission Symp., Japan Soc. NDI, Tokyo, pp. 429-442.

Teoh, H.B. and Kanji Ono (1987), J. Acoustic Emission, **6**(1), 1-12.